ANTICANCER RESEARCH *38*: 4449-4457 (2018)
doi:10.21873/anticanres.12747

Quantitative Structure–Cytotoxicity Relationship of Pyrano[4,3-*b*]chromones

JUNKO NAGAI[1], HAIXIA SHI[2,3], YUKA KUBOTA[4], KENJIRO BANDOW[5], NORIYUKI OKUDAIRA[6], YOSHIHIRO UESAWA[1], HIROSHI SAKAGAMI[2], MINEKO TOMOMURA[5], AKITO TOMOMURA[5], KOICHI TAKAO[4] and YOSHIAKI SUGITA[4]

[1]Department of Medical Molecular Informatics, Meiji Pharmaceutical University, Tokyo, Japan;
[2]Department of Traditional Chinese Medicine, Shanghai Ninth People's Hospital, Shanghai Jiatong University School of Medicine, Shanghai, P.R. China;
[3]Meikai University Research Institute of Odontology (M-RIO), Saitama, Japan;
[4]Department of Pharmaceutical Sciences, Faculty of Pharmacy and Pharmaceutical Sciences, Josai University, Saitama, Japan;
Divisions of [5]Biochemistry and [6]Pharmacology, Meikai University School of Dentistry, Saitama, Japan

Abstract. *Background/Aim: 4H-1-Benzopyran-4-one (chromone) provides a backbone structure for the chemical synthesis of potent anticancer drugs. Since studies of the biological activity of pyrano[4,3-b]chromones are limited, we investigated a total of 20 pyrano[4,3-b]chromones (10 sets of diastereomers) for their cytotoxicity against four human oral squamous cell carcinoma (OSCC) cell lines and human normal oral cells, and then carried out a quantitative structure–activity relationship (QSAR) analysis. Materials and Methods: Cytotoxicity was determined by the 3-(4,5-dimethylthiazol-2-yl)-2,5-diphenyltetrazolium bromide method. Tumor-specificity (TS) was evaluated by the ratio of mean 50% cytotoxic concentration (CC_{50}) against normal oral cells to that against human OSCC cell lines. Potency-selectivity expression (PSE) value was calculated by dividing the TS value by the CC_{50} against tumor cells. Apoptosis induction was evaluated by morphological observation, western blot analysis and cell-cycle analysis. For QSAR analysis, a total of 3,072 physicochemical, structural and quantum chemical features were calculated from the most stabilized structure optimized using CORINA. Results: 8-Chloro-4,4a-dihydro-3-methoxy-3-methyl-3H,10H-pyrano[4,3-b][1]benzopyran-10-one (**16**) and 3-ethoxy-4,4a-dihydro-8-methoxy-3H,10H-pyrano[4,3-b][1]benzopyran-10-one (**17**) had the highest TS, higher than that of 5-flurouracil and melphalan, without induction of apoptosis. Compound **16** induced cytostatic growth inhibition and much lower cytotoxicity against human normal oral keratinocytes compared to doxorubicin. TS of 20 pyrano[4,3-b]chromones was correlated with 3D structure, polarity, ionic potential and electric state. Conclusion: Chemical modification of **16** may be a potential choice for designing a new type of anticancer drug.*

Correspondence to: Yoshihiro Uesawa, Department of Medical Molecular Informatics, Meiji Pharmaceutical University, 2-522-1 Noshio, Kiyose, Tokyo 204-858, Japan. Tel/Fax: +81 424958983, e-mail: uesawa@my-pharm.ac.jp

Key Words: Pyrano[4,3-*b*]chromones, QSAR analysis, cytotoxicity, tumor selectivity, keratinocyte toxicity, apoptosis induction, molecular shape.

Using 4*H*-1-Benzopyran-4-one (chromone), found ubiquitously in the plant kingdom (1), as a backbone structure, we synthesized 3-styrylchromones (2), 3-styryl-2*H*-chromenes (3) and 2-azolylchromones (4), and found them to have much higher cytotoxicity against human oral squamous cell carcinoma (OSCC) cell lines than against human normal oral mesenchymal cells (gingival fibroblast, periodontal ligament fibroblast, pulp cells). These compounds were relatively less cytotoxic against human oral keratinocytes as compared with common anticancer drugs (5).

As far as we know, studies of the biological activity of pyrano[4,3-*b*]chromones have been limited to the identification of new compounds from marine fungus (6), binding affinity to human opioid receptors (subtypes δ, κ, and μ) and cannabinoid receptors (CB1 and CB2) (7), and their antimicrobial activity (8). In continuation of discovering new biological activities of chromone derivatives, we investigated a total of 20 pyrano[4,3-*b*]chromones (10 pairs of diastereomers) (A-series **1-10** and B-series **11-20** in Figure 1) for their cytotoxicity against four human OSCC cell lines and three human normal oral cell types, and then subjected them to quantitative structure–activity relationship (QSAR) analysis.

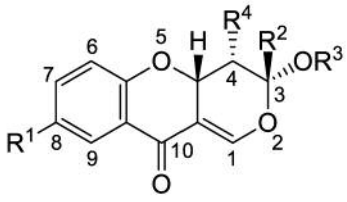

A: 1-10

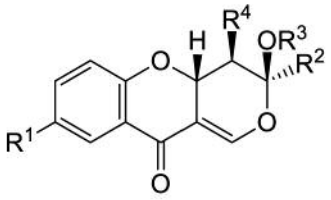

B: 11-20

Compound					
A	**B**	R^1	R^2	R^3	R^4
1	**11**	H	H	Et	H
2	**12**	H	H	Bu	H
3	**13**	H	Me	Me	H
4	**14**	Cl	H	Et	H
5	**15**	Cl	H	Bu	H
6	**16**	Cl	Me	Me	H
7	**17**	OMe	H	Et	H
8	**18**	OMe	H	Bu	H
9	**19**	OMe	Me	Me	H
10	**20**	H	H	$-(CH_2)_3-$	

Figure 1. *Structure of 20 pyrano[4,3-b]chromones investigated in this study.*

Materials and Methods

Materials. The following chemicals and reagents were obtained from the indicated companies: Dulbecco's modified Eagle's medium (DMEM) from GIBCO BRL (Grand Island, NY, USA); fetal bovine serum (FBS), 3-(4,5-dimethylthiazol-2-yl)-2,5-diphenyltetrazolium bromide (MTT), melphalan, doxorubicin, ribonuclease (RNase) A from Sigma-Aldrich Inc. (St. Louis, MO, USA); 5-fluorouracil (5-FU) from Kyowa (Tokyo, Japan); propidium iodide (PI), dimethyl sulfoxide (DMSO), actinomycin D, 4% paraformaldehyde phosphate buffer solution from Wako Pure Chem. Ind. (Osaka, Japan); Nonidet-P40 (NP-40) from Nakalai Tesque Inc. (Kyoto, Japan); and culture plastic dishes and 96-well plates from Techno Plastic Products AG (Trasadingen, Switzerland).

Synthesis of pyrano[4,3-b]chromone derivatives. Diastereomer pairs of 3-ethoxy-4,4a-dihydro-3*H*,10*H*-pyrano[4,3-*b*][1]benzopyran-10-one (**1, 11**), 3-butoxy-4,4a-dihydro-3*H*,10*H*-pyrano[4,3-*b*][1]benzopyran-10-one (**2, 12**), 4,4a-dihydro-3-methoxy-3-methyl-3*H*,10*H*-pyrano[4,3-*b*][1]benzopyran-10-one (**3, 13**), 8-chloro-3-ethoxy-4,4a-dihydro-3*H*,10*H*-pyrano[4,3-*b*][1]benzopyran-10-one (**4, 14**), 3-butoxy-8-chloro-4,4a-dihydro-3*H*,10*H*-pyrano[4,3-*b*][1]benzopyran-10-one (**5, 15**), 8-chloro-4,4a-dihydro-3-methoxy-3-methyl-3*H*,10*H*-pyrano[4,3-*b*][1]benzopyran-10-one (**6, 16**), 3-ethoxy-4,4a-dihydro-8-methoxy-3*H*,10*H*-pyrano[4,3-*b*][1]benzopyran-10-one (**7, 17**), 3-butoxy-4,4a-dihydro-8-methoxy-3*H*,10*H*-pyrano[4,3-*b*][1]benzopyran-10-one (**8, 18**), 4,4a-dihydro-3,8-dimethoxy-3-methyl-3*H*,10*H*-pyrano[4,3-*b*][1]benzopyran-10-one (**9, 19**), and 2,3,12a,12b-tetrahydro-1*H*,4a*H*,7*H*-pyrano[3',2':5,6]pyrano[4,3-*b*][1]benzopyran-7-one (**10, 20**) were synthesized by the cycloaddition reactions of 3-formylchromones with selected enol ethers, according to previous methods (9). All compounds were dissolved in DMSO at 40 mM and stored at –20˚C before use.

Cell culture. Human normal oral mesenchymal cells (human gingival fibroblast, HGF; human periodontal ligament fibroblast, HPLF) were established from the first premolar tooth extracted from the lower jaw of a 12-year-old girl (10), and cells at 10-18 population doubling levels were used in this study. Human oral OSCC cell lines (Ca9-22, derived from gingival tissue); HSC-2, derived from tongue) were purchased from Riken Cell Bank (Tsukuba, Japan). All of these cells were cultured at 37˚C in DMEM supplemented with 10% heat-inactivated FBS, 100 units/ml, penicillin G and 100 μg/ml streptomycin sulfate under a humidified 5% CO_2 atmosphere. Human oral keratinocyte (HOK) cells (purchased from Cosmo Bio Co. Ltd., Tokyo, Japan) were cultured in keratinocyte growth supplement (OKGS, Cat, No. 2652; CliniSciences, Nanterre, France) and cells at 7-11 population doubling levels were used in the present study. Cell morphology was checked periodically under a light microscope (EVOS FL; Thermo Fisher Scientific, Waltham, MA, USA).

Assay for cytotoxic activity. Cells were inoculated at 2×10^3 cells/0.1 ml in a 96-microwell plate. After 48 h, the medium was replaced with 0.1 ml of fresh medium containing different concentrations of single test compounds. Cells were incubated for a further 48 h and the relative viable cell number was then determined by the MTT method (2-5). The relative viable cell number was determined from the absorbance of the cell lysate at 560 nm, using a microplate reader (Infinite F50R; TECAN, Männedorf, Switzerland). Control cells were treated with the same amounts of DMSO and the cell damage induced by DMSO was subtracted from that induced by test agents. The concentration of compound that reduced the viable cell number by 50% (CC_{50}) was determined from the dose–response curve and the mean value of CC_{50} for each cell type was calculated from triplicate assays.

Calculation of tumor-specificity index (TS). TS was calculated using the following equation: TS=mean CC_{50} against normal oral cell types/mean CC_{50} against OSCC cell lines. Since both Ca9-22 and HGF cells were derived from gingival tissue (11), the relative sensitivity of these cells was also compared (as: mean CC_{50} against HGF/mean CC_{50} against Ca9-22).

Table I. *Cytotoxic activity of 20 pyrano[4,3-b]chromones against oral malignant and non-malignant cells. Each value represents the mean of triplicate determinations. Two sets of tumor-specificity index (TS) and potency-selectivity expression (PSE) values were determined using all oral squamous cell carcinoma (OSCC) compared with non-malignant cells, and paired cells derived from the same (gingival) tissue.*

	Human OSCC cell lines					Human normal oral cells					TS		PSE	
Compound	Ca9-22 (A)	SD	HSC-2	SD	Mean (B)	HGF (C)	SD	HPLF	SD	Mean (D)	(D/B)	C/A)	$(D/B^2)\times100$	$(C/A^2)\times100$
1	194	13	369	53	282	>400	0	>400	0	>400	>1.4	>2.1	>0.5	>1.1
2	105	9	187	3	146	>400	0	>387	22	>394	>2.7	>3.8	>1.9	>3.7
3	28	4	32	0	30	245		270	28	257	8.6	8.7	28.7	31.2
4	313	103	>400	0	>357	>400	0	>400	0	>400	><1.1	>1.3	><0.3	>0.4
5	74	5	237	142	155	>400	0	>400	0	>400	>2.6	>5.4	>1.7	>7.3
6	33	2	41	3	37	142	28	192	51	167	4.6	4.3	12.4	13.2
7	142	10	175	22	158	>400	0	>398	4	>399	>2.5	>2.8	>1.6	>2.0
8	84	7	221	43	153	>391	16	>400	0	>396	>2.6	>4.6	>1.7	>5.5
9	12	0	15	1	14	88	10	103	31	95	7.0	7.1	51.6	57.1
10	68	1	95	18	82	347	33	246	19	297	3.6	5.1	4.4	7.5
11	103	12	115	20	109	340	15	273	6	307	2.8	3.3	2.6	3.2
12	42	2	75	7	58	288	43	244	10	266	4.5	6.9	7.8	16.5
13	16	1	24	8	20	175	9	125	8	150	7.6	11.2	38.6	72.0
14	52	5	93	4	73	294	4	146	108	220	3.0	5.7	4.2	10.9
15	21	2	43	3	32	182	7	240	60	211	6.6	8.5	20.5	39.5
16	4.7	1.4	5.3	0.4	5	247	41	233	20	240	47.8	52.6	953.0	1118.2
17	11.1	0.6	13.9	4.2	12	>386	24	318	18	>352	>28.2	>34.9	>225.9	>315.4
18	35	8	76	14	56	316	19	285	52	300	5.4	9.1	9.7	26.1
19	15	1	15	1	15	142	31	117	32	129	8.6	9.5	57.2	63.8
20	137	6	267	16	202	>397	6	391	37	>394	>1.9	>2.9	>1.0	>2.1
5-FU	31	2	198	65	115	>1000		>1000	0	>1000	>8.7	31.8	>7.6	101.2
Melphalan	29	5	10	1	20	182	3	182	17	182	9.2	6.2	46.9	21.4
DXR	0.33	0.15	0.08	0.01	0.21	>10		>10	0.00	>10	>48.5	>30.4	>23488.8	>9220.0

HGF: Human gingival fibroblast; HPLF: human periodontal ligament fibroblast; CC_{50}: 50% cytotoxic concentration; DXR: doxorubicin; 5-FU, 5-fluorouracil; Ca9-22, Derived from gingival tissue; HSC-2, HSC-3 and HSC-4, derived from tongue.

Calculation of potency-selectivity expression (PSE). PSE was calculated by the following equation: PSE=mean CC_{50} against normal oral cell types/(CC_{50} against OSCC cell lines)^2 ×100 (HGF, HPLF *vs*. Ca9-22, HSC-2); and as mean CC_{50} against HGF/(CC_{50} against Ca9-22)^2 ×100 using the pair of cell types from the same tissue (gingiva) (see Table I).

Western blot analysis. Cells were washed with phosphate-buffered saline (PBS) and re-suspended in 50 mM Tris-HCl (pH 7.6), 150 mM NaCl, 1 mM EDTA, 0.1% sodium dodecyl sulfate (SDS), 0.5% deoxycholic acid, 1% NP-40 and protease inhibitors (RIPA buffer). After ultrasonication using Bioruptor (UCD-250; Cosmo Bio) for 12.5 min (10 s on, 20 s off) at 250 W at 4˚C, the soluble cellular extracts were recovered after centrifugation for 10 min at 16,000 × *g*. The protein concentration of each sample was determined using BCA Protein Assay Reagent Kit (Thermo Fisher Scientific) and cell extracts were subjected to western blot analysis. The blots were probed with anti-poly (ADP-ribose) polymerase (PARP) (Cell Signaling Technology Inc., Beverly, MD, USA), anti-caspase 3 (Cell Signaling Technology Inc.), or anti-glyceraldehyde 3-phosphate dehydrogenase (GAPDH) (Trevigen, Gaithersburg, MD, USA), followed by a horseradish peroxidase-conjugated anti-α-rabbit IgG secondary antibody (DAKO, Glostrup, Denmark). The immune complexes were visualized using Pierce Western Blotting Substrate Plus (Thermo Fisher Scientific). Western blotting results were documented and quantified using ImageQuant LAS 500 (GE Healthcare, Tokyo, Japan) (12).

Cell-cycle analysis. Treated and untreated cells (approximately 10^6 cells) were harvested, fixed with 1% paraformaldehyde in PBS without calcium and magnesium ions [PBS(−)]. Fixed cells were then washed twice with PBS(−), and treated for 30 min with 400 μl of 0.2 mg/ml RNase A (preheated for 10 min at 100˚C to inactivate DNase) to degrade RNA. Cells were then washed twice with PBS(−) and stained for 15 min with 0.01% PI in the presence of 0.01% NP-40 in PBS(−) to prevent cell aggregation. After filtering through Falcon® cell strainers (40 μM) (Corning, NY, USA) to remove aggregated cells, PI-stained cells were subjected to cell sorting (SH800 Series; SONY Imaging Products and Solutions Inc., Kanagawa, Japan). Cell-cycle analysis was performed with Cell Sorter Software version 2.1.2. (SONY Imaging Products and Solution Inc.).

Estimation of CC_{50} values. Since the CC_{50} values had a distribution pattern close to a logarithmically normal distribution, we used the negative log CC_{50} (pCC_{50}) values for the comparison of cytotoxicity between compounds. The mean pCC_{50} values for normal cells and tumor cell lines were defined as N and T, respectively (3).

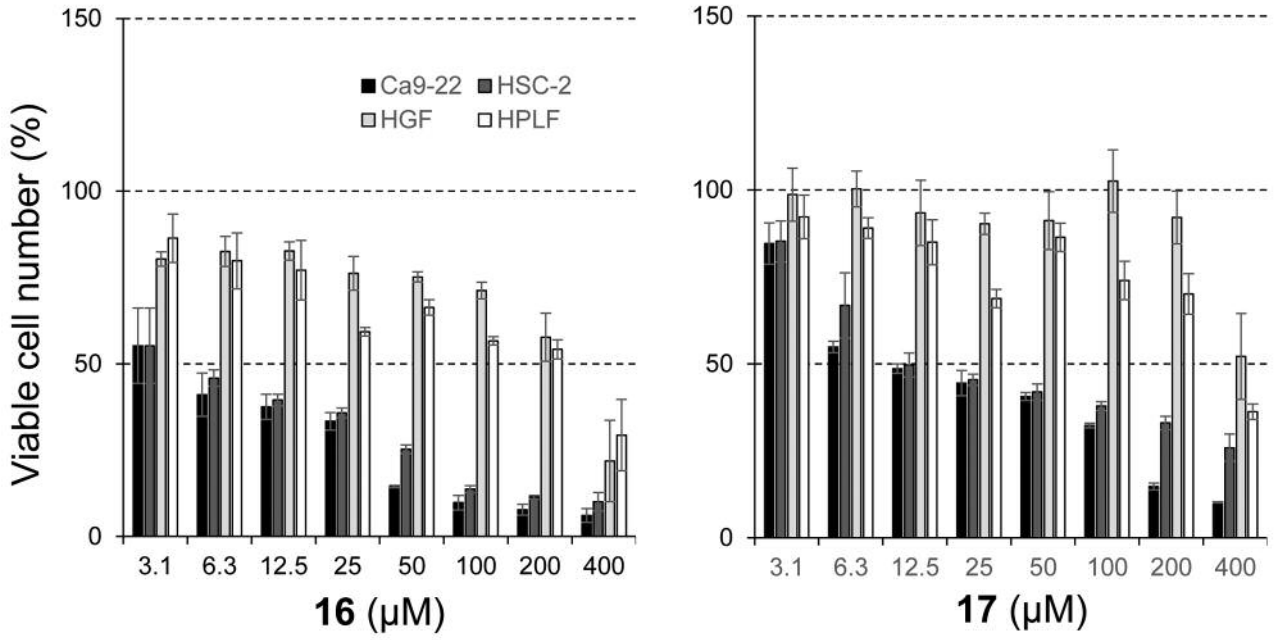

Figure 2. *Cytotoxicity of compounds **16** and **17** against human oral squamous cell carcinoma cell lines Ca9-22 and HSC-2, and human normal oral cells, human gingival fibroblast (HGF) and human periodontal ligament fibroblast (HPLF). Cells were incubated for 48 h without (control) or with the indicated concentrations of **16** or **17**, and cell viability was determined by MTT method, and expressed as a percentage that of the control. Each value represents the mean±S.D. of triplicate assays.*

Calculation of chemical descriptors. The 3D structure of each chemical structure (Marvin Sketch ver 16; ChemAxon, Budapest, Hungary, http://www.chemaxon.com) was optimized by CORINA Classic (Molecular Networks GmbH, Nürnberg, Germany) with forcefield calculations (amber-10: EHT) in Molecular Operating Environment (MOE) version 2018.0101 (Chemical Computing Group Inc., Quebec, Canada). The number of structural descriptors calculated from MOE (13) and Dragon 7.0 (14) (Kode srl., Pisa, Italy) was 344 and 5,255, respectively. Among them, the number of descriptors used for analysis was 290 and 2,782 (total 3,072), respectively.

Statistical treatment. The CC_{50} values were expressed as mean±S.D. of triplicate assays. The relation among cytotoxicity, TS and chemical descriptors were investigated using simple regression analyses by JMP Pro version 13.2.0 (SAS Institute Inc., Cary, NC, USA). The significance level was set at $p<0.05$.

Results

Cytotoxicity. A total of 20 pyrano[4,3-*b*]chromone derivatives, consisting of 10 pairs of diastereomers were synthesized (A-series **1-10** and B-series **11-20** in Figure 1).

Replacement of ethoxy group at the C-3 position with butoxy or methoxy and methyl group increased the cytotoxicity of most of these compounds, as evidenced by decreasing CC_{50} values: 282→146→30 (**1-3**), >357→155→37 (**4-6**), 158→153→14 (**7-9**), 109→58→20 (**11-13**), 73→32→5 μM (**14-16**) in OSCC cells (Table I), and >400→>394→257 (**1-3**), >400→>400→167 (**4-6**), >399→>396→95 μM (**7-9**) in human normal oral cells (Table I). The replacement effects were more pronounced against OSCC cell lines than normal oral cells.

Table II. *Toxicity of compound **16** against human oral keratinocytes (HOK) and human oral squamous cell carcinoma (OSCC) cell lines as compared with doxorubicin.*

	CC_{50} (mM)		
	OSCC	HOK	TS
16	5	20.3	4.1
Doxorubicin	0.21	0.119	0.6

CC_{50}: 50% Cytotoxic concentration; TS: tumor-specificity.

The replacement of ethoxy with additional pyran moiety (**10, 20**), and the introduction of chlorine or methoxyl group (**1-3** *vs*. **4-6** or **7-9**; **11-13** *vs*. **14-16** or **17-19**) only slightly affected cytotoxicity (Table I).

Tumor specificity. Among the 20 compounds, **16** had the highest TS (TS=47.8), followed by **17** (TS>28.2). The TS value of other compounds was below 10. TS value of **16** was slightly higher than that of 5-FU and melphalan, and comparable with that of doxorubicin (Table I).

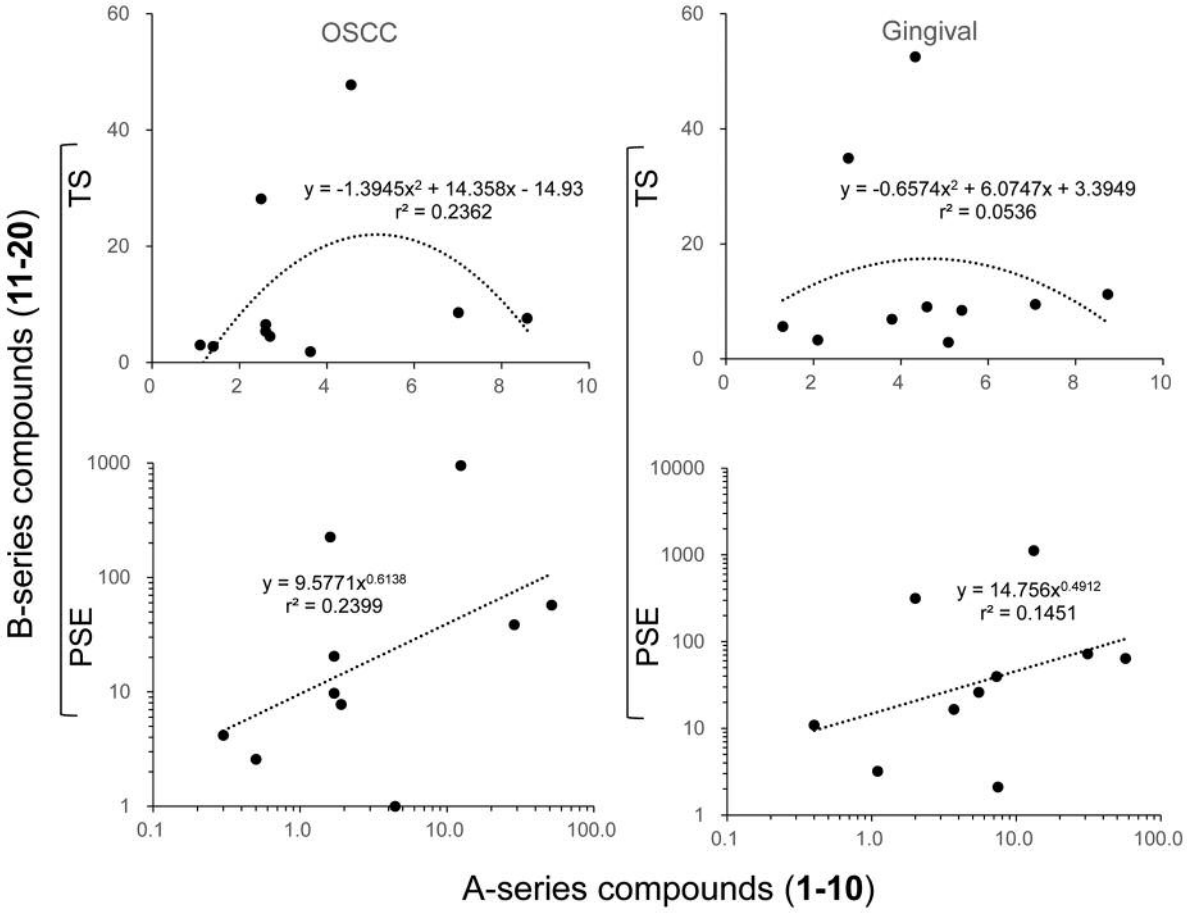

Figure 3. *Correlation of tumor-specificity (TS) and potency-selectivity expression (PSE) for diastereomer pairs from A (**1-10**) and B (**11-20**) series of compounds, plotted per pair: (**1**, **11**), (**2**, **12**), (**3**, **13**), (**4**, **14**), (**5**, **15**), (**6**, **16**), (**7**, **17**), (**8**, **18**), (**9**, **19**) and (**10**, **20**). Fitted curves or lines and r2 values were calculated by Microsoft Excel (Windows 10, Microsoft Corporation, Redmond, WA, USA). Correlations are shown for TS and PSE values for all oral squamous cell carcinoma (OSCC) cell lines versus non-malignant cells (left), and paired cells derived from the same (gingival) tissue (right).*

Considering that HGF is the normal cell corresponding to Ca9-22 OSCC cell line (since both derive from gingival tissues), TS values were also calculated by dividing the average CC_{50} value towards HGF cells by the CC_{50} value towards Ca9-22 cells (C/A, Table I). The TS values derived in this way for **16** (TS=52.6) and **17** (TS>34.9) were higher than that of melphalan but comparable with those of 5-FU and doxorubicin (Table I).

Compounds **16** and **17** showed cytostatic growth inhibition of OSCC cells (Figure 2). Cytotoxicity of **16** against human oral keratinocytes was approximately 14% of that of doxorubicin (Table II).

PSE. In order to identify the most promising compounds in terms of both good potency and selectively cytotoxicity, the PSE values were calculated. PSE values of **16** and **17** (953.0 and >225.9, respectively) against malignant cells were 125- and 30-fold higher, respectively, than that of 5-FU and 20- and 5-fold higher, respectively, than that of melphalan. For gingival tissue, PSE values of **16** and **17** (1,118.2 and >315.4) were 11-and 3-fold higher, respectively, than that of 5-FU, and 52 and 15-fold higher, respectively, than that of melphalan (Table I). However, PSE values of **16** and **17** was one order lower than that of doxorubicin (Table I).

There was weak correlation between TS for all malignant cells, and for gingival cells (r^2=0.2362 and 0.0536, respectively) and PSE values (r^2=0.2399 and 0.1451, respectively) between each pair of diastereomers (Figure 3).

*Type of cell death induced by **16***. When HSC-2 cells were incubated for 24 h with increasing concentrations (5, 10, 20, 40, 80 μM) of **16**, cells became gradually enlarged. In contrast, actinomycin D treatment induced cell shrinkage, characteristic of apoptosis (Figure 4A). A shorter incubation time (24 h) was

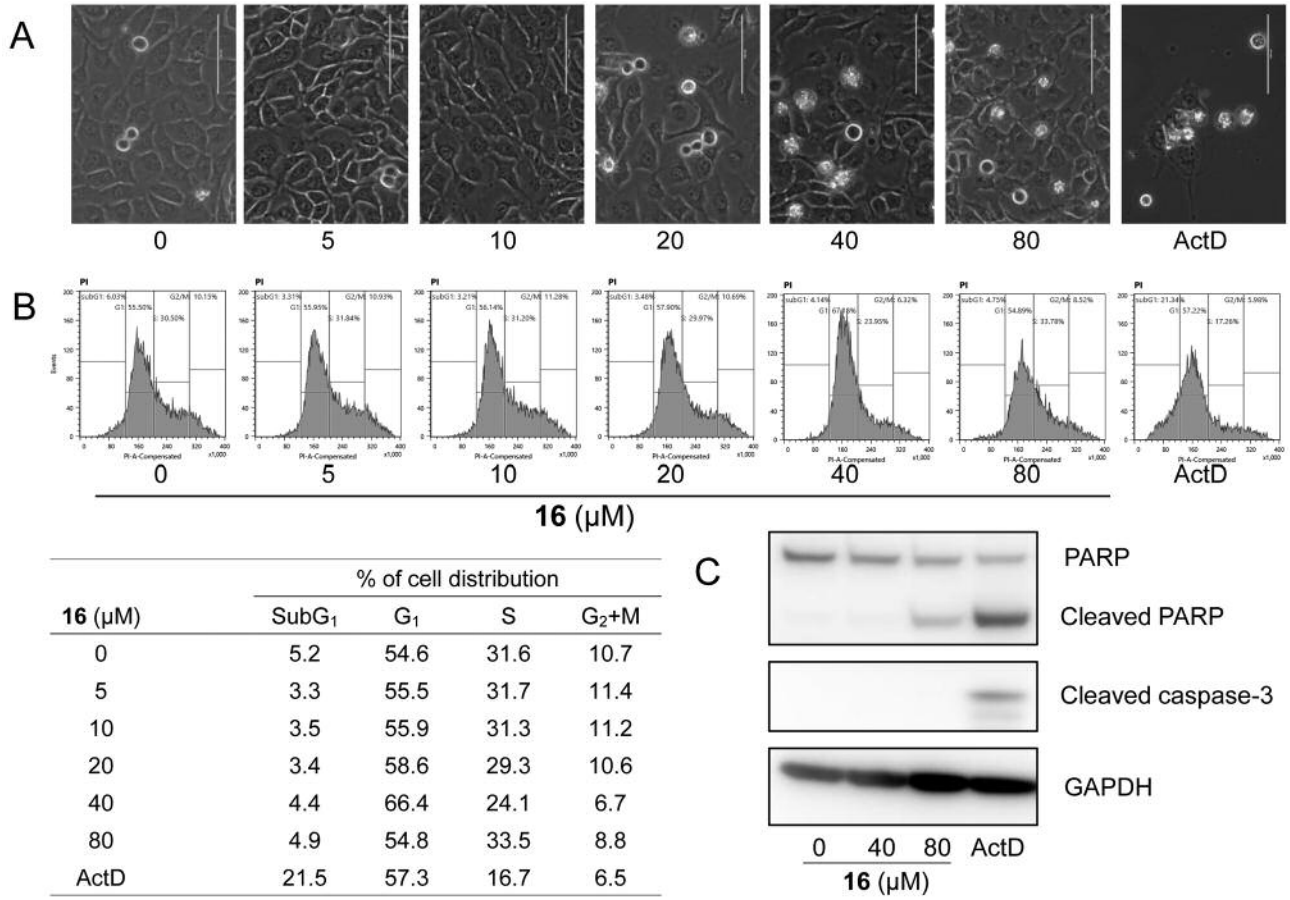

	% of cell distribution			
16 (μM)	$SubG_1$	G_1	S	G_2+M
0	5.2	54.6	31.6	10.7
5	3.3	55.5	31.7	11.4
10	3.5	55.9	31.3	11.2
20	3.4	58.6	29.3	10.6
40	4.4	66.4	24.1	6.7
80	4.9	54.8	33.5	8.8
ActD	21.5	57.3	16.7	6.5

Figure 4. *Effect of compound **16** on cell morphology (A), cell-cycle distribution (B) and expression of apoptosis-related proteins (C) in oral squamous cell carcinoma cell line HSC-2. Cells were incubated for 24 h with the indicated concentrations of **16** or 1 μM actinomycin D (Act D) as positive control and then assessed for morphology under light microscopy (EVOS FL; Thermo Fisher Scientific), cell-cycle distribution by cell sorting and apoptosis induction by western blot. Bar=100 μm. GAPDH: Glyceraldehyde 3-phosphate dehydrogenase, PARP: poly (ADP-ribose) polymerase.*

used to detect early changes in cellular metabolism. This caused the difference in the viable cell number between the control and treated cells detected by MTT method to be much smaller.

Cell-cycle analysis demonstrated that actinomycin D, but not **16**, produced a sub-G_1 cell population that is characteristic of apoptotic cells (Figure 3B). The percentage of G_2+M phase cells was gradually reduced (from 10.7% to as low as 6.7%, similar to the level with actinomycin D), as concentrations of **16** increased (Figure 4B).

Western blot analysis demonstrated that **16** did not lead to caspase-3 activation, as evidenced by lack of cleavage of PARP and capspase-3, in contrast to actinomycin D treatment (Figure 4C). These data suggest that **16** did not induce apoptosis.

Computational analysis. We next performed the QSAR analysis of 20 pyrano[4,3-*b*]chromones in regards to their cytotoxicity against tumor cells and normal cells. Since 554, 638 and 130 chemical descriptors were significantly ($p<0.05$) correlated with cytotoxicity against tumor cells, cytotoxicity against normal cells, and TS (data not shown), we chose the top six chemical descriptors for QSAR analysis (Figures 5, 6 and 7, and Table III).

The cytotoxicity of 20 pyrano[4,3-*b*]chromones derivatives against human OSCC cell lines was positively correlated with descriptors R8s (3D shape, size and electric state) ($r^2=0.661$, $p<0.0001$), J_G (3D shape) ($r^2=0.607$, $p<0.0001$), RDF055s (3D shape and electric state) ($r^2=0.595$, $p<0.0001$), R7s (3D shape, size and electric state) ($r^2=0.570$, $p=0.0001$), HATS7s (3D shape, size and electric state) ($r^2=0.556$, $p=0.0002$) and RTs (3D shape, size and electric state) ($r^2=0.552$, $p=0.0002$) (Figure 5).

The cytotoxicity of 20 pyrano[4,3-*b*]chromones derivatives against human normal oral mesenchymal cells was correlated positively with R6v+ (3D shape and size) ($r^2=0.768$, $p<0.0001$), R1s (3D shape, size and electric state) ($r^2=0.658$, $p<0.0001$), R4v (3D shape and size) ($r^2=0.656$, $p<0.0001$), J_G ($r^2=0.651$, $p<0.0001$), R4p (3D shape, size and

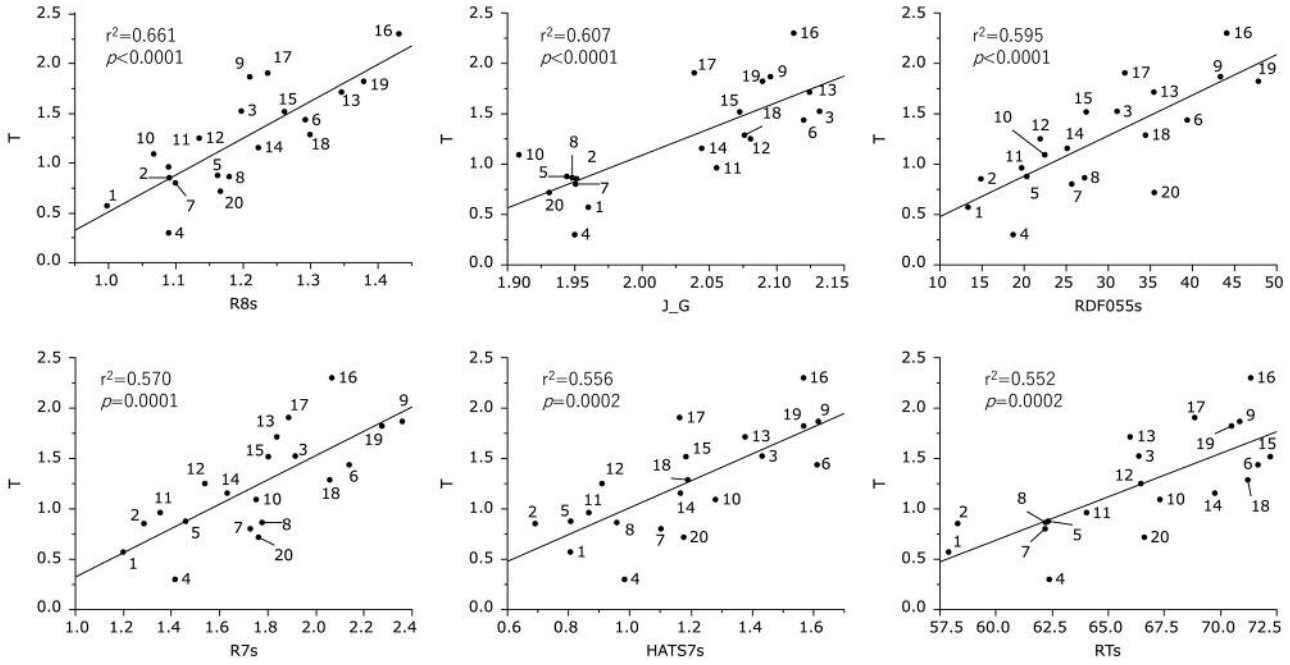

Figure 5. *Determination of correlation coefficient between chemical descriptors and cytotoxicity of 20 pyrano[4,3-b]chromones against tumor cells. The mean values of the negative log of the concentration of compound that reduced the viable cell number by 50% (CC_{50}) (T) against tumor cells were plotted. CC_{50}: Concentration of compound that reduced the viable cell number by 50%. The following chemical descriptors were used: HATS7s, R7s, R8s, RTs: 3D shape, size and electric state; J_G: 3D shape; RDF055s: 3D shape and electric state.*

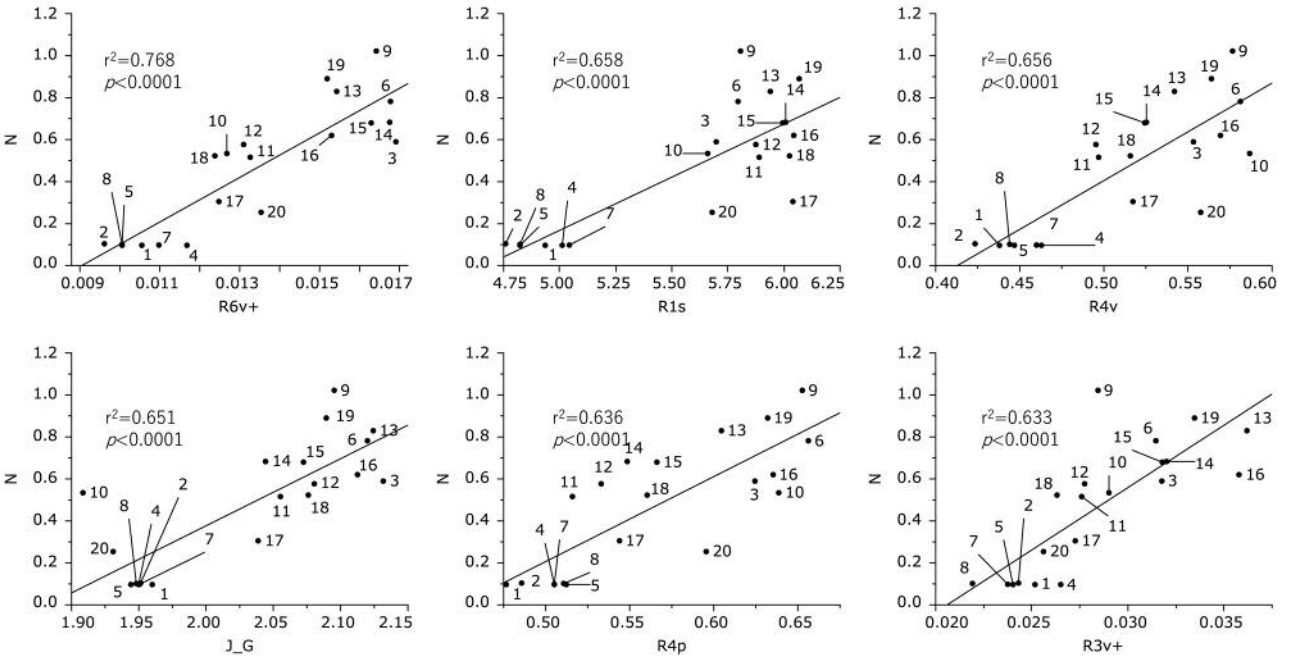

Figure 6. *Determination of correlation coefficient between chemical descriptors and cytotoxicity of 20 pyrano[4,3-b]chromones against normal cells. The mean values of the negative log of the concentration of compound that reduced the viable cell number by 50% (CC_{50}) (N) against normal cells were plotted. The following chemical descriptors were used: R3v+, R4v, R6v+: 3D shape and size; R1s: 3D shape, size and electric state; J_G: 3D shape; and R4p: 3D shape, size and polarizability.*

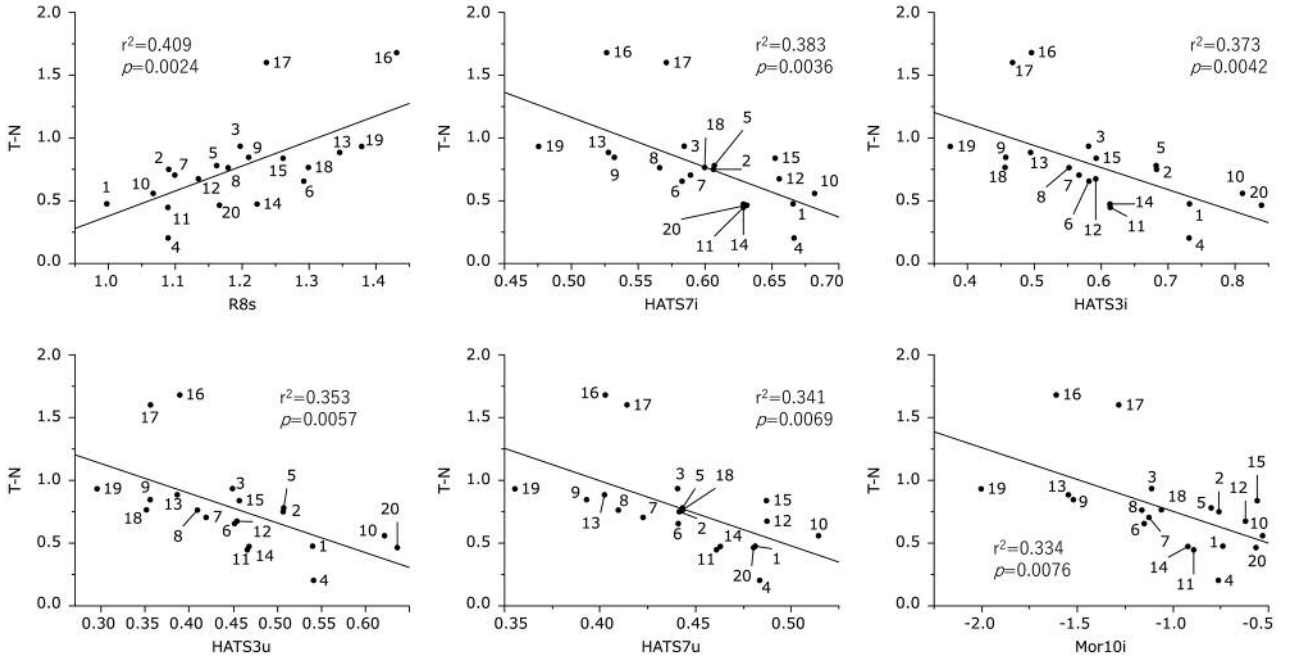

Figure 7. *Determination of coefficient between chemical descriptors and tumor specificity of 20 pyrano[4,3-b]chromones [defined as: cytotoxicity against tumor cells−cytotoxicity against normal cells (T−N)]. The following chemical descriptors were used: R8s: 3D shape, size and electric state; HATS3i, HATS7i, 3D shape, size and ionization potential; HATS3u, HATS7u: 3D shape and size; Mor10i: 3D shape and ionitation potential.*

Table III. *Properties of descriptors that significantly affected cytotoxicity against tumor cells (T) and normal cells (N), and tumor specificity (T−N).*

	Descriptor	Source	Meaning	Explanation
T	R8s	Dragon	3D shape, size and electric state	Autocorrelation of lag 8/weighted by I-state
	J_G	Dragon	3D shape	Balaban-like index from geometrical matrix
	RDF055s	Dragon	3D shape and electric state	Radial Distribution Function-055/weighted by I-state
	R7s	Dragon	3D shape, size and electric state	R autocorrelation of lag 7/weighted by I-state
	HATS7s	Dragon	3D shape, size and electric state	Leverage-weighted autocorrelation of lag 7/weighted by I-state
	RTs	Dragon	3D shape, size and electric state	R total index/weighted by I-state
N	R6v+	Dragon	3D shape and size	R maximal autocorrelation of lag 6/weighted by van der Waals volume
	R1s	Dragon	3D shape, size and electric state	R autocorrelation of lag 1/weighted by I-state
	R4v	Dragon	3D shape and size	R autocorrelation of lag 4/weighted by van der Waals volume
	J_G	Dragon	3D shape	Balaban-like index from geometrical matrix
	R4p	Dragon	3D shape, size and polarizability	R autocorrelation of lag 4/weighted by polarizability
	R3v+	Dragon	3D shape and size	R maximal autocorrelation of lag 3/weighted by van der Waals volume
T−N	R8s	Dragon	3D shape, size and electric state	R autocorrelation of lag 8/weighted by I-state
	HATS7i	Dragon	3D shape, size and ionization potential	Leverage-weighted autocorrelation of lag 7/weighted by ionization potential
	HATS3i	Dragon	3D shape, size and ionization potential	Leverage-weighted autocorrelation of lag 3/weighted by ionization potential
	HATS3u	Dragon	3D shape and size	Leverage-weighted autocorrelation of lag 3/unweighted
	HATS7u	Dragon	3D shape and size	Leverage-weighted autocorrelation of lag 7/unweighted
	Mor10i	Dragon	3D shape and ionization potential	Signal 10/weighted by ionization potential

polarizability) (r^2=0.636, p<0.0001), and R3v+ (3D shape and size) (r^2=0.633, p<0.0001) (Figure 6).

The TS of pyrano[4,3-*b*]chromones derivatives was positively correlated with R8s (r^2=0.409, p=0.0024), and negatively with HATS7i (3D shape, size and ionization potential) (r^2=0.383, p=0.0036), HATS3i (3D shape, size and ionization potential) (r^2=0.373, p=0.0042), HATS3u (3D shape and size) (r^2=0.353, p=0.0057), HATS7u (3D shape

and size) (r^2=0.341, p=0.0069), and Mor10i (3D shape and ionization potential) (r^2=0.334, p=0.0076) (Figure 7).

Discussion

The present study demonstrated, for the first time, that among 20 pyrano[4,3-*b*]chromones derivatives, **16** and **17** had the highest tumor specificity (as shown by TS and PSE values), greater than that of 5-FU and melphalan, comparable to that of doxorubicin (Table I). Both **16** and **17** led to cytostatic growth inhibition (Figure 2). It is possible that the presence of the methoxy and methyl group at the C-3 position and chlorine at the C-8 position increased the cytotoxicity of **16** against OSCC cell lines. On the other hand, the presence of the methoxy group at the C-8 position may contribute to increasing the tumor specificity of **17**. We confirmed our previous finding that doxorubicin showed potent cytotoxicity against human normal oral keratinocyte cells (5), and that **16** was much less cytotoxic against HOK than doxorubicin (Table II), suggesting that this compound may be an attractive compound for further research.

We found that **16** did not produce a G_1 cell population nor did it induce caspase-3 activation, suggesting that **16** does not induce apoptotic cell death. This suggests that there may be no connection between the tumor specificity and apoptosis-inducing activity. There are a variety of types of cell death reported (15). Further study is needed to determine which type of cell death **16** induces in human OSCC cell lines.

QSAR analysis demonstrated that cytotoxicity of 20 pyrano[4,3-*b*]chromones derivatives against tumor cell lines was significantly positively correlated (p<0.002) with descriptors of 3D shape, size and electric state (Figure 5). Their tumor specificity was also significantly positively correlated (p=0.0024-0.0076) with 3D shape, size and electric state, and negatively correlated with 3D shape, size and ionization potential (Figure 7). Chemical modification using **16** as a lead compound may be a potential choice for designing a new type of anticancer drug.

Conflicts of Interest

The Authors wish to confirm that there are no known conflicts of interest associated with this publication and there has been no significant financial support for this work that could have influenced its outcome.

Acknowledgements

This work was partially supported by KAKENHI from the Japan Society for the Promotion of Science (JSPS) (15K08111, 16K11519).

References

1 Gaspar A, Matos MJ, Garrido J, Uriarte E and Borges F: Chromone: a valid scaffold in medicinal chemistry. Chem Rev *114(9)*: 4960-4992, 2014.

2 Shimada C, Uesawa Y, Ishii-Nozawa R, Ishihara M, Kagaya H, Kanamto T, Terakubo S, Nakashima H, Takao K, Sugita Y and Sakagami H: Quantitative structure–cytotoxicity relationship of 3-styrylchromones. Anticancer Res *34*: 5405-5412, 2014.

3 Uesawa Y, Sakagami H, Ishihara M, Kagaya H, Kanamoto T, Terakubo S, Nakashima H, Yahagi H, Takao K and Sugita Y: Quantitative structure–cytotoxicity relationship of 3-styryl-2*H*-chromenes. Anticancer Res *35*: 5299-5308, 2015.

4 Sakagami H, Okudaira N, Uesawa Y, Takao K, Kagaya H and Sugita Y: Quantitative structure-cytotoxicity relationship of 2-azolylchromones. Anticancer Res *38(2)*: 763-770, 2018.

5 Sakagami H, Okudaira N, Masuda Y, Amano O, Yokose S, Kanda Y, Suguro M, Natori T, Oizumi H and Oizumi T: Induction of apoptosis in human oral keratinocyte by doxorubicin. Anticancer Res *37(3)*: 1023-1029, 2017.

6 Cheng X, Yu L, Wang Q, Ding W, Chen Z and Ma Z: New brefeldins and penialidins from marine fungus *Penicillium janthinellum* DT-F29.Nat Prod Res *32(3)*: 282-286, 2018.

7 León F, Gao J, Dale OR, Wu Y, Habib E, Husni AS, Hill RA and Cutler SJ: Secondary metabolites from *Eupenicillium parvum* and their *in vitro* binding affinity for human opioid and cannabinoid receptors. Planta Med *79(18)*: 1756-1761, 2013.

8 Kaur A, Sharma V, Budhiraja A, Kaur H, Gupta V, Kant R and Mohan Ishar MP: Synthesis and evaluation of substituted 4,4a-Dihydro-3*H*,10*H*-pyrano[4,3-*b*][1]benzopyran-10-one as antimicrobial agent. ISRN Med Chem *2013*: ID619535, 2013.

9 Saengchantara ST and Wallace TW: Heterodiene cycloadditions of 3-acylchromones with enol ethers. J Chem Soc Perkin Trans I *1986*: 789-794, 1986.

10 Kantoh K, Ono M, Nakamura Y, Nakamura Y, Hashimoto K, Sakagami H and Wakabayashi H: Hormetic and anti-radiation effects of tropolone-related compounds. In Vivo *24*: 843-852, 2010.

11 Horikoshi M, Kimura Y, Nagura H, Ono T and Ito H: A new human cell line derived from human carcinoma of the gingiva. I. Its establishment and morphological studies. Jpn J Oral Maxillofac Surg *20*: 100-106, 1974.

12 Tomikoshi Y, Nomura M, Okudaira N, Sakagami H and Wakabayashi H: Enhancement of cytotoxicity of three apoptosis-inducing agents against human oral squamous cell carcinoma cell line by benzoxazinotropone. In Vivo *30(5)*: 645-650, 2016.

13 Calculate Descriptors, MOE2018.01 on-line help manual, Chemical Computing Group. https://www.chemcomp.com/MOE2018.htm

14 https://chm.kode-solutions.net/products_dragon_descriptors.php

15 Fricker M, Tolkovsky AM, Borutaite V, Coleman M and Brown GC: Neuronal cell death. Physiol Rev *98(2)*: 813-880, 2018.

Received June 8, 2018
Revised July 1, 2018
Accepted July 5, 2018